The Solution Structure of BmTx3B, a Member of the Scorpion Toxin Subfamily α-KTx 16

Yuefeng Wang,[†] Xiang Chen,[†] Naixia Zhang, Gong Wu, and Houming Wu*
State Key Laboratory of Bio-Organic and Natural Products Chemistry, Shanghai Institute of Organic Chemistry, Chinese Academy of Sciences, Shanghai, P. R. China

ABSTRACT **This article reports the solution structure of BmTx3B (α-KTx16.2), a potassium channel blocker belonging to the subfamily α-KTx16, purified from the venom of the Chinese scorpion *Buthus martensi* Karsch. In solution, BmTx3B assumes a typical CSαβ motif, with an α-helix connected to a triple-stranded β-sheet by 3 disulfide bridges, which belongs to the first structural group of short-chain scorpion toxins. On the other hand, BmTx3B is quite different from other toxins (such as ChTx and AgTx2) of this group in terms of the electrostatic and hydrophobic surface distribution. The functional surface (β-face) of the molecule is characterized by less basic residues (only 2: Lys28 and Arg35) and extra aromatic residues (Phe1, Phe9, Trp15, and Tyr37). The peptide shows a great preference for the Kca1.1 channel over the Kv channel (about a 10^3-fold difference). The model of BmTx3B/Kca1.1 channel complex generated by docking and dynamic simulation reveals that the stable binding between the BmTx3B and Kca1.1 channel is favored by a number of aromatic π–π stacking interactions. The influences of these structural features on the kinetic behavior of the toxin binding to Kca1.1 channel are also discussed. Proteins 2005;58:489–497.**

Key words: BmTx3B; *Buthus martensi* Karsch; Kv channel; Kca1.1 channel; NMR solution structure; potassium channel blocker

INTRODUCTION

Scorpion venoms contain a large diversity of neurotoxins that bind to various ion channels at the surface of excitable cells and modify their physiological properties. According to their activities and specific targets, these toxins are divided into different classes: (1) long-chain toxins (60–76 amino acid residues with 4 disulfide bonds) that target specifically voltage-gated sodium channels,[1] and (2) short-chain neurotoxins (30–40 amino acid residues cross-linked by 3–4 disulfide bridges) that act mainly on various potassium channels.[2,3] Recently the literature on scorpion toxins that specifically interact with various potassium channels has increased rapidly. To date, 19 subfamilies of the channel blockers have been identified.[4–6] Ever-increasing molecular data on the 3D structures of novel scorpion toxins and K^+ channels reveal a variety of novel interacting modes between these toxins and channels.[7–11] The knowledge of the interacting surface between the toxins and channels should help increase our understanding of the K^+ channel structure and function relationships.

The Chinese scorpion *Buthus martensi* Karsch (BmK) has been used as traditional medicine in China for more than 1000 years, especially for the treatment of neural diseases, such as apoplexy, hemiplegia, and facial paralysis.[12] During the past few years, a number of peptides have been identified and characterized from the venom of BmK by systematic isolation, ESI-MS, N-terminal sequence, and toxicity.[13] However, only a few solution structures of scorpion peptide toxins have been reported.[6,14–18]

BmTx3B (also named Martentoxin, or BmK 622, in the previous literature) is a 37–amino acid toxin purified from the venom of the Chinese scorpion BmK. BmTx3B was initially thought to belong to subfamily 1 (α-KTx1.12) but recently has been classified as a toxin belonging to subfamily 16 (α-KTx16.2).[7,10] The sequence alignment of BmTx3B with other short-chain scorpion toxins (Fig. 1) clearly indicated that the homology of BmTx3B with those of TmTx (α-KTx16.1)[19] and Lqh15-1 (α-KTx16.3)[20] is high (73% and 75%, respectively), but is quite low (39% and 44%, respectively) as compared with those of ChTx (α-KTx1.1)[21] and IbTx (α-KTx1.3).[22] In electrophysiological studies, this peptide showed a great preference for Kca1.1 channel over Kv channel (a 10^3-fold difference). BmTx3B inhibited the delayed rectifying potassium current (I_K) in rat hippocampal neurons, with very low potency (at micromole levels).[23] On the contrary, the peptide could selec-

Abbreviations: 1D, one dimensional; 2D, two dimensional; 3D, three dimensional; BmK, *Buthus martensi* Karsch; DQF-COSY, double-quantum-filtered shift correlated spectroscopy; DSS, 2,2-dimethylsilapentane-5-sulfonate; EM, energy minimization; ESI-MS, electrospray ionization mass spectrometry; HERG, human *ether-a-go-go*-related gene; Kca1.1 channel, high-conductance calcium-activated potassium channel; Kv channel, voltage-gated potassium channel; NOE, nuclear Overhauser effect; NOESY, nuclear Overhauser enhancement spectroscopy; REM, restrained energy minimization; RMSD, root-mean-square deviation; TOCSY, total correlation spectroscopy.

[†]These authors contributed equally to this work.

Grant sponsor: National Science Foundation of China; Grant number: 20132030. Grant sponsor: Chinese Academy of Sciences; Grant number: KGCX2-SW-213-05.

*Correspondence to: Houming Wu, Shanghai Institute of Organic Chemistry, Chinese Academy of Sciences, Shanghai, 200032, P.R. China. E-mail: hmwu@mail.sioc.ac.cn

Received 11 May 2004; Accepted 26 July 2004

Published online 19 November 2004 in Wiley InterScience (www.interscience.wiley.com). DOI: 10.1002/prot.20322

```
          1         10         20         30      37  identity
BmTx3B    FGLIDVKCFASSECWTACKKVTGSGQGKCQNNQCRCY-      100%
Lqh 15-1  -GLIDVRCYDSRQCWIACKKVTGSTQGKCQNKQCRCY-     75.7%
TmTX      -DLIDVKCISSQECWIACKKVTGRFEGKCQNRQCRCY-     73.0%
IbTX      -ZFTDVDCSVSKECWSVCKDLFGVDRGKCMGKKCRCYQ     44.7%
ChTX      -ZFTNVSCTTSKECWSVCQRLHNTSRGKCMNKKCRCYS     39.5%
```

Fig. 1. Sequence alignment of BmTx3B with that of Lqh 15-1, TmTx, IbTx, and ChTx. The amino acid sequences are aligned according to their cysteine residues.

tively block Kca1.1 channel currents (IC_{50}: 21 n*M*).[24] To the best of our knowledge, no 3D structure of toxins from this subfamily has been reported yet. To reveal the structural features of this subfamily and clarify the determinants for the affinity toward Kca1.1 channel, the solution structure of BmTx3B and model of BmTx3B/Kca1.1 channel complex are investigated in this article.

MATERIALS AND METHODS

NMR Sample Preparation

The BmTx3B sample was isolated and purified from the venom of Chinese scorpion BmK (purity ~99%).[13] The characterization, amino acid composition analysis, and sequence determination of this toxin (the name originally used is BmK622) were reported in the previous article.[25]

NMR Experiments

For the NMR experiments, 5.0 mg of the peptide sample was used. The solvents used were either 100% D_2O or a mixture of 90% H_2O and 10% D_2O (v/v). The pH was adjusted to 3.0 by adding 1 μL of dilute DCl or NaOD, and the final concentration of BmTx3B was about 2.5 m*M*.

All the NMR experiments were recorded at 303 K on a Varian unity Inova 600 spectrometer. Spectra were referenced to sodium DSS. Quadrature detection was employed in all experiments, and the carrier frequency was always maintained at the solvent resonance. Presaturation was used to suppress the water peak in all experiments. DQF-COSY, TOCSY, and NOESY spectra were recorded in a phase-sensitive mode. All the 2D spectra were acquired with 2 K data points (4 K for DQF-COSY) in t_2 dimension and 512 data points in t_1 dimension. TOCSY spectra were recorded using the MLEV-17 pulse sequence with a spin lock period of 30, 50, and 80 ms, respectively. NOESY spectra were obtained with 3 different mixing times: 100, 200, and 300 ms, respectively. Shifted sine window function and zero filling were applied prior to Fourier transformation. For determination of slowly exchanging amide protons, a series of 1D spectra in first 4 h and then 2 TOCSY spectra (mixing time, 80 ms, 6 h) were recorded at 303 K immediately after the sample was redissolved in 100% D_2O. The experimental data were acquired and processed using the Vnmr 6.1B program on a SUN Sparc Station 4 computer. The processed data were analyzed using XEASY for visualization of NMR spectra, peak picking, and peak integration on a Silicon Graphics Indigo II R 5000 computer.

Assignment Strategy and Structure Calculation

The identification of amino acid spin systems and the sequential assignment were achieved using the standard strategy described by Wüthrich.[26]

The NOESY (200 ms) spectrum was used to generate the distance constraints. Dihedral angle constraints were derived from $^3J_{HNH\alpha}$ on the basis of DQF-COSY spectra. Additional constraints were used to enforce hydrogen bonds implicated by H–D exchange spectra. The structures were calculated using DYANA on a silicon graphic Indigo II computer, and then were subjected to REM using the AMBER 5.0 package. The 25 best DYANA conformers with the lowest free energy were used to represent the solution conformation of BmTx3B. The programs PROCHECK and PROCHECK_NMR were used to analyze the NMR structures of BmTx3B. In addition, for visual comparison of the structures, 3D conformations were produced with the molecular graphics program MOLMOL on a silicon graphic indigo II computer. For pairs of conformers, superposition and RMSD values for various subsets of atoms were calculated. The mean solution structure was obtained by superimposing the 25 lowest energy DYANA conformers and then averaging the Cartesian coordinates of the corresponding atoms in the 25 superimposed conformers, and followed by energy minimization.

Docking of BmTx3B on a Model of Kca1.1

The model of the Kca1.1 channel[27] was generated by homology modeling on the basis of the crystal structure of the bacterial KcsA channel[28] using the software SYBYL6.3 (Tripos Associates, 1996). The sequence alignment between KcsA and Kca1.1 channel was obtained using the same criteria as those described by Gao and Garcia.[29] The homology model of Kca1.1 was further subjected to Powell minimization (2000 steps) using the Kollman force field.

The surface electrostatic distribution analysis indicated that BmTx3B preferred association with the entryway of K^+ channels using the positively charged patch located at the β-sheet with the side-chains of Lys28 as the center.

The program "O" (version 8.0.6)[30] was used for the docking experiment. BmTx3B was docked manually into the outer entryway of the Kca1.1 channel model along with the dipole direction. As expected, the mouth of the K^+ channel bears a large negative charge, whereas the surface of BmTx3B toxin has a positive charge. The electrostatic potential between the BmTx3B toxin and K^+ channels attracted the positively charged toxin to the entryway of the channel. In order to obtain favorable toxin–channel

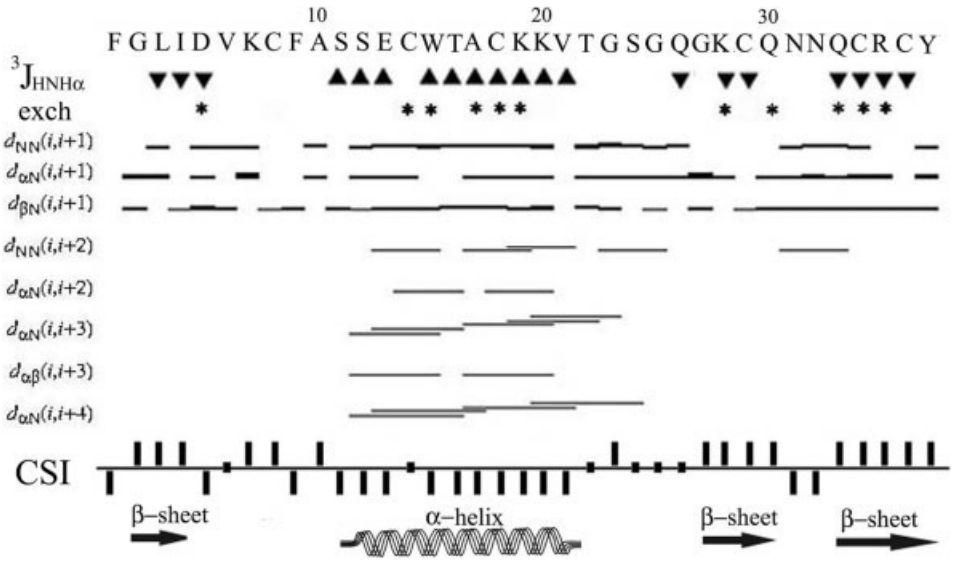

Fig. 2. Summary of NOE connectivities, J-coupling constant $^3J_{HNH\alpha}$, the amide proton exchange rate, and C$^\alpha$H chemical shift index. The thickness of the bar indicates the intensity of NOEs. Stars represent the NH protons in slowly exchanging. J-coupling constant $^3J_{HNH\alpha}$ are smaller than 6.5 Hz (▲) and bigger than 8 Hz (▼). Positive bars and negative bars in the chemical shift index indicate the C$^\alpha$H protons downfield and upfield shifted by $>$ 0.1 ppm, respectively, as compared with the C$^\alpha$H proton chemical shifts of random-coil. The derived secondary structures based on NMR parameters are shown at the bottom.

clusters, the toxin molecule was allowed to rotate during the docking process. The most stable cluster with the best fit between toxin and K^+ channel was used to analyze the contacts between BmTx3B and the K^+ channel.

The peptide/K^+-channel clusters that docked most favorably were further subjected to energy minimization for 2000 steps to achieve the gradient tolerance 0.05 kcal/(mol Å) using the Powell algorithm and the Kollman force field in the software SYBYL6.3. Molecular dynamics simulation using the Powell algorithm was then carried out for these complexes for 100 fs at 300 K. Kollman force field constraints were applied on the backbones of the channel in the region comprising residues His254 to Val278, while the remaining part of the channel was kept fixed during the simulation. The structures of the peptides were completely unconstrained. A cutoff distance of 8 Å was used for nonbounded interactions. An integration timestep of 0.1 fs was used, and coordinate sets of the trajectory were saved every 2 fs. Every structure obtained from the coordinate sets over the 100 fs of simulation was performed with 500 steps of minimization. Finally, the average structure was energy minimized with 1000 steps of Powell minimization.

RESULTS

NMR Resonance Assignment

The sequence-specific resonance assignment of BmTx3B was achieved according to the general procedure developed by Wüthrich.[26] First, the spin systems were identified by their scalar connectivities on the basis of DQF-COSY and TOCSY spectra. The fingerprint region of DQF-COSY spectra recorded in H_2O showed most of the HN-Hα cross-peaks expected, and the TOCSY spectra were used to correlate these H_N-H_α cross-peaks with their side-chain spin systems. In the second assignment step, the spin systems were connected in sequence by the virtue of $d_{\alpha N}$, d_{NN}, and $d_{\beta N}$ connectivities in well-dispersed NOESY spectra. The unique residues Trp15 and Tyr37 in BmTx3B were used as the entrance points for sequential assignments. Starting from these 2 amino acids, the assignment proceeds smoothly both in forward and reverse directions via $d_{\alpha N}$, d_{NN}, and $d_{\beta N}$ connectivities. Complete sequential assignments were achieved, and the results are summarized in Figure 2. In addition, the medium-range NOE contacts such as $d_{\alpha N}(i, i + 3)$, $d_{\alpha\beta}(i, i + 3)$, $d_{\alpha N}(i, i + 4)$, and $d_{\alpha N}(i, i + 2)$, the coupling constants $^3J_{HNH\alpha}$, and the slowly exchanging amide protons (NH/ND), as well as the chemical shift index of the α-protons are also summarized in Figure 2.

Hydrogen Bonds

Amide protons, which were still visible after 10-h of exchanging, were considered to be engaged with hydrogen bonds (Fig. 2). Most of the slowly exchanged amide protons occurred in regular secondary structures such as HN14, 15, 17, 18, 19 in the helix and HN28, 30, 33, 34 in the β-sheet, and their acceptors of hydrogen bonds were identified during the structure refinement.

Coupling Constants

Twenty-six $^3J_{HNH\alpha}$ coupling constants were measured by the well-dispersed 1D ^1H NMR and DQF-COSY spectra. Eleven missing $^3J_{HNH\alpha}$ values were attributed to 4 Gly residues (2, 23, 25 and 27), and 5 other residues due to the peak overlap in the DQF-COSY spectrum, as well as the N-terminal and C-terminal residues. Of the 26 coupling constants, 20 belonging to regular secondary struc-

ture (α-helix and β-sheet) were converted into torsion angle restraints.

Secondary Structure

Secondary structural elements of BmTx3B were identified using the unique NOESY connectivities and $^3J_{HNH\alpha}$ coupling constants. A continuous set of $d_{NN}(i, i + 1)$ NOEs were observed in the segment from Ser11 to Lys20, which is indicative of a helical conformation in this region. The deduction was supported by a serial of medium-range NOEs, such as $d_{\alpha N}(i, i + 3)$ and $d_{\alpha N}(i, i + 4)$. Further corroborative data came from $^3J_{HNH\alpha}$ coupling constants and slowly exchanging amide protons. Most of the $^3J_{HNH\alpha}$ coupling constants in this region (except Cys14) are smaller than 7.0 Hz. All the amide protons in the region of Ala17–Lys19 are slow in exchanging (Fig. 2). Besides, the chemical shifts of α-protons in this secondary element move upfield. These data further confirmed the above assignment of the helical structure.

On the other hand, strands Gly27–Gln30 and Gln33–Cys36 showed strong sequential $d_{\alpha N}$ connectivities and large $^3J_{HNH\alpha}$ (> 8.0 Hz) coupling constants. Meanwhile, a network of long-range $d_{\alpha N}$, $d_{\alpha\alpha}$ and d_{NN} NOEs, such as $d_{\alpha\alpha}$ (27, 36), $d_{\alpha\alpha}$ (29, 34), $d_{\alpha N}$ (29, 35), $d_{\alpha N}$ (30, 34), $d_{\alpha N}$ (36, 28), d_{NN} (28, 35), and d_{NN} (30, 33) were observed for these 2 strands. These observations suggested the presence of a double-stranded β-sheet in these regions. These 2 strands were connected by a type I β-turn (residues 30–33). In addition, on the basis of a number of long-range NOEs between segments Gly2–Ile4 and Gln33–Cys36, as well as the hydrogen bond between Cys36 and Gly2, the segment Gly–Ile 4 also runs antiparallel to strands Gln33–Cys36. The location of the triple-stranded antiparallel β-sheet was confirmed by the chemical shift index of the α-protons and the slowly exchanging amide proton data. As shown in Figure 2, all the amide protons of the central strand were slowly exchanged, whereas the amide protons of 2 external strands exhibited a typical alternating pattern of rapid and slow exchange rates. The hydrogen-bond partner of amide proton of Cys36 was identified as being the carbonyl oxygen of Gly2.

Structure Determination

The input for distance geometry calculations with the program DYANA consisted of upper distance limits derived from NOESY (mixing time 200 ms) cross-peak intensities by the program CALIBA, and dihedral angle constraints obtained from an initial interpretation of the vicinal coupling constants $^3J_{HNH\alpha}$. For the calibration of proton–proton distance limits (r vs the cross-peak intensities), the dependence of $1/r^6$ was used for all protons. These calibration curves were refined based on plotting cross-peak volume versus average proton–proton distance according to the preliminary structures. A total of 523 distance constraints were used: 225 intraresidue, 136 sequential, 76 medium-range ($1 < |i - j| \leq 4$), and 86 long-range ($|i - j| > 4$). Twenty φ angle constraints ($-60 \pm 30°$ for $^3J_{HNH\alpha} < 7.0$ Hz and $-120 \pm 40°$ for $^3J_{HNH\alpha} > 8.0$ Hz) were obtained using the program HABAS from the 1D ^{1}H spectrum and DQF-COSY in H_2O. In addition, 9 distance constraints were added for 3 disulfide bonds (3 per bond). Nine hydrogen-bond constraints were imposed between slow-exchanging amide protons and their receptors based on the DYANA preliminary structures. For each hydrogen bond, 2 limit restraints were used between the NH–O (0.22 nm) and the N–O (0.32 nm) atom pairs. In addition, the program GLOMSA was used to obtain 5 stereo-specific assignments of β-methylene protons on the basis of the preliminary structures. Totally, 570 constraints (an average of 15 constraints per residue) were obtained and used in structure calculations.

The structures were calculated using program DYANA on a Silicon Graphic Indigo II computer. Starting from 300 random structures, 30 preliminary structures with lowest target functions resulting from distance geometry calculations were subjected to simulated annealing and REM using the SANDER module of AMBER 5.0 package. A cutoff radius of 0.8 nm for nonbonded interactions, with a residue-based pair-list routine, was used in all calculations. The force constants for distance restraints in EM calculations were 500 kJ mol^{-1} nm^{-2}. EM was performed using a combination of steepest descent and conjugate gradient algorithms with a gradient convergence norm of less than 10^{-4} kJ mol^{-1} nm^{-1}. After energy minimization with AMBER, the 25 best DYANA conformers with the lowest energy are used to represent the solution conformation of BmTx3B.

Structure Description

Figure 3 shows the superposition of the polypeptide backbones of 25 best conformers. No distance violations larger than 0.10 Å and no angle violations larger than 5° could be found. The overall agreement among individual conformers is indicated by global RMSD. The final set of 25 structures shows an overall RMSD of 0.65 Å for the backbone atoms and 1.49 Å for all heavy atoms. The RMSD values for backbone atoms and the heavy atoms are changed to 0.35 Å and 1.15 Å, respectively, when the first 2 residues and the last residue of the toxin are not taken into consideration. The secondary structures are defined much better by RMSD values of 0.19 Å and 0.28 Å, respectively, for the backbone atoms of the α-helix and β-sheet. The structural statistics of the final set of structures are summarized in Table I. Analysis of the ensemble of 25 structures using PROCHECK_NMR reveals that 98.7% of the residues lie in the most favored and allowed regions of the Ramachandran ϕ, ψ dihedral angle plot (not shown).

The mean structure of BmTx3B is obtained from the best 25 conformers [Fig. 4(a)]. The molecule adopts the α/β-scaffold, which consists of a triple-stranded antiparallel β-sheet anchored to a single α-helix (Ser11–Val21) by 3 disulfide bridges (C8–C29, C14–C34, and C18–C36). The β-sheet involves residues Gly2–Ile4 (strand I), Gly27–Gln30 (strand II), and Gln33–Cys36 (strand III); the latter 2 strands are connected by a type I turn (residues 30–33). The comparison of the global folding of the molecule with those of other toxins in this structural group is shown in Figure 4(b).

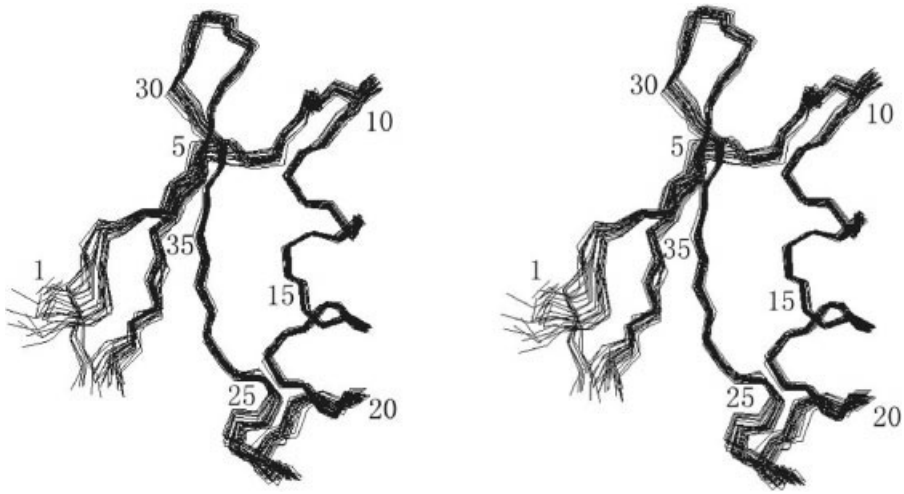

Fig. 3. Stereoview for backbone superimposition of the best 25 structures of BmTx3B; each fifth residue is numbered.

TABLE I. Constraint Statistics and Structural Analysis for the Best 25 Conformers of BmTx3B

Constraints statistic	
Distance constraints	
Intraresidue	225
Sequential ($\|i - j\| = 1$)	136
Medium range ($1 < \|i - j\| < 5$)	76
Long range ($\|i - j\| > 5$)	86
H-bonds	18
Constraints for disulfide bridge	9
All	550
Dihedral angle constraints	
ϕ angle constraints	20
RMSD versus the mean structure (Å)	
All backbone atoms	0.65
All heavy atoms	1.49
Backbone atoms (residues 3–36)	0.35
Heavy atoms (residues 3–36)	1.15
Structure analysis (%)	
Residues in most favored regions	77.5
Residues in allowed regions	19.8
Residues in generously allowed regions	1.4
Residues in disallowed regions	1.3

Interaction of BmTx3B With Kca1.1 Channel

The structural model of BmTx3B–Kca1.1 channel complex is shown in Figure 5(a). It clearly demonstrated that the solvent-exposed surface of β-sheet containing positively charged residues Lys28 and Arg35 was involved in the electrostatic interactions with potassium channel. The most favorable docked conformation was found with the intimate contacts between Lys28 and Tyr290 (I–IV), Trp15 and Phe266 (I), Ser11 and Gly291 (II), Asn31 and Gln270 (III), and Arg35 and Asp292 (IV), as well as Tyr37 and Phe266 (IV) [Fig. 5(b)].

The principal interactions between BmTx3B and Kca1.1 channel derived from the refined complex structure were analyzed using the LIGPLOT program and the results are summarized in Table II.[33] Totally, 12 hydrogen bonds, 1 salt bridge, and 10 hydrophobic contacts existed in the refined complex. Therefore, the interface between BmTx3B and Kca1.1 channel is large and involves about 9 residues of BmTx3B and 18 residues of the Kca1.1 channel, respectively, as shown in Figure 5(c).

DISCUSSION

The solution structure of BmTx3B and the model of BmTx3B–Kca1.1 channel complex are investigated in this article to reveal the structural features and to evaluate interaction interface of BmTx3B with Kca1.1 channel.

Structural Features of BmTX3B

According to Possani and coworkers,[7] two different structural groups of toxins have been documented. The first group, including α-KTx subfamilies 1–4, 6, 7, and 12, and the γ-KTx subfamily 2, contains a triple-stranded β-sheet and either 3 or 4 disulfide bridges. The second group, which includes α-KTx subfamilies 5, 8, 9, and 13, is characterized by an N-terminal deletion with respect to the first group, which results in lack of the first strand of the β-sheet. BmTx3B, which possesses a common αβ -motif and a triple-stranded antiparallel β-sheet, thus belongs to the first group. Actually, it exhibits high similarity in the 3D structure to other short-chain toxins in this structural group, as shown in Figure 4(b).

On the other hand, BmTx3B is quite different from other toxins (such as ChTx, AgTx2, and NTx) of this group in terms of electrostatics and hydrophobic surface distribution. Gao and Garcia[29] reported that ChTx binds to Kv channel or Kca1.1 channel using its β-surface of the hairpin structure, and the functional map contains Lys27 as the center, which is surrounded by residues Ser10, Arg25, Met29, Asn30, Arg34, Trp14, and Tyr36 [Fig. 5(d)]. This interface is characterized by a number of positively charged residues: Besides Arg25, Lys27, and Arg34 mentioned above, residues Lys11 and Lys31 are also involved in this surface. The latter 2 basic residues may take part in

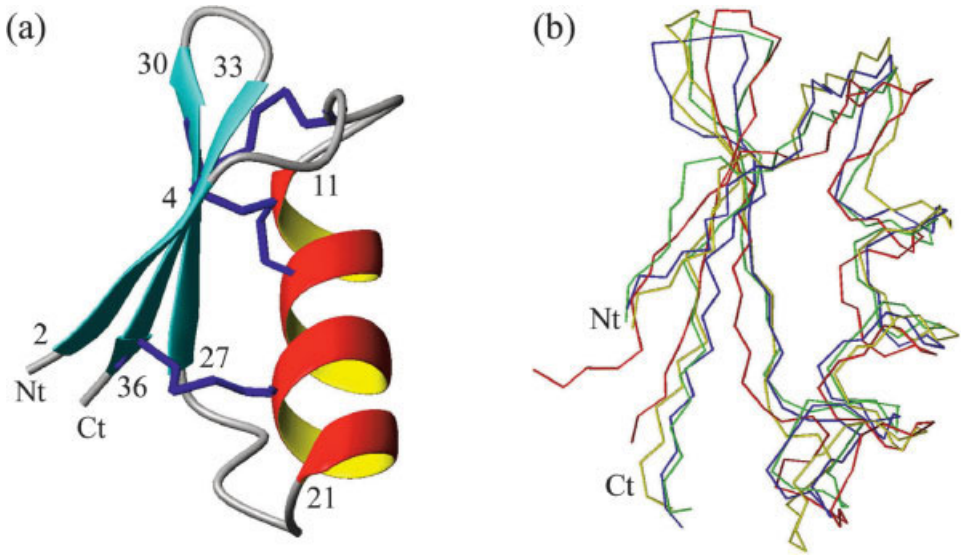

Fig. 4. (**a**) MOLMOL representation of the mean structure of BmTx3B. Secondary structural elements are drawn with 3 disulfide bridges (blue). Beginning and ending residues of each secondary structure elements are labeled according to protein sequence. (**b**) Superposition of the backbone of BmTx3B (red) with ChTx (yellow) (2CRD),[31] BmTx2 (blue) (2BMT),[14] and Lq2 (green) (1LIR).[32] Nt and Ct indicate N-terminus and C-terminus, respectively.

the recognition and correct positioning of the toxin on the channel despite the fact that they may not be involved in the final interactions of the toxin with the channel. As pointed out by Sabatier and coworkers,[34] these basic residues may form a basic ring in toxin binding. In addition, the interface is unique in that several hydrogen bond–forming residues, such as Ser11, Met29, and Asn30, lie at the central region within 5.5 Å of Lys27.

In contrast, in BmTx3B, the β-face of the hairpin structure contains fewer basic residues, only 2: Lys28 and Arg35. Remaining basic residues of the molecule, Lys19 and Lys20 (both in the α-helix), as well as Lys7, are located at the second surface of the molecule (referred to as the α-face). Meanwhile, compared with ChTx, the β-face of BmTx3B contains fewer hydrogen bond–forming residues, only 2 (Ser11 and Asn31), without a Met residue in the central region, which is crucial for the pore block binding. In addition, the β-face of BmTx3B is characterized by a number of aromatic residues: Phe1, Phe9, Trp15, and Tyr37, while only 2 aromatic residues (Trp14 and Tyr36) appear at the relevant position in ChTx toxin. These unique structural features should have an important influence on the selectivity of the toxin to the target channels and on the interaction mode therein.

Interaction of BmTx3B With the Kca1.1 Channel

BmTx3B could selectively block Kca1.1 channel with the IC_{50} of 21 n*M*, which is more potent by 10^3 times than that toward the Kv channel. Thus, what is the determinant for the higher affinity of BmTx3B toward the Kca1.1 channel?

As shown in the interaction interface [Fig. 5(a–c, and e)] of BmTx3B with the Kca1.1 channel, the positively charged side-chain of Lys28 lies in the center of the peptide–channel complex to form hydrogen bonds with the 4 backbone carbonyls of Tyr290. Ser11 and Asn31 form hydrogen bonds with the residues Gly291 (II) and Gln270 (III) of Kca1.1 channel, respectively, while Arg35 salt-bridges with Asp292 (IV). Meanwhile, the model of BmTx3B–Kca1.1 complex demonstrates a distinctive feature due to a number of aromatic interactions. Tyr37 forms favorable aromatic contacts with Phe266 (IV) and Tyr294 (IV) of the Kca1.1 channel, while Trp15 of BmTx3B forms aromatic contacts with Phe266 (I) and Tyr294 (I). In addition, residue Phe1 and Phe9 appear to form aromatic contacts with Phe266 (IV) and Phe266 (II) of the channel, respectively [Fig. 5(e)]. Therefore, the overall binding of BmTx3B with Kca1.1 channel is stabilized by a number of aromatic interactions. These results accounted well for the higher affinity of BmTx3B binding with Kca1.1 channel.

The Determinant for the Affinity of BmTx3B to Kca1.1 Channel

The architecture of Kca1.1 and Kv1.3 channels in the pore region appears to be similar, and the main difference is observed in the S5 outer loop.[29] The sequence Pro372-Thr373-Ser374-Gly375 of the S5 outer loop of the Kv1.3 channel has to align with the sequence Phe266-Gln267-Asn268-Asn269-Gln270 of Kca1.1. It is clear that the residue Phe266 of Kca1.1 channel is beneficial to forming the aromatic contacts. Actually, the aromatic residues Phe1 and Phe9 of BmTx3B form extra aromatic contacts with Phe266 (IV) and Phe266 (II), respectively, in the BmTx3B–Kca1.1 complex. Furthermore, it is worth pointing out that the role of the aromatic residues cannot be attributed to hydrophobicity alone. Miller and coworkers[35] reported that the mutation of Tyr36 in ChTx by residue Leu or Ala resulted in

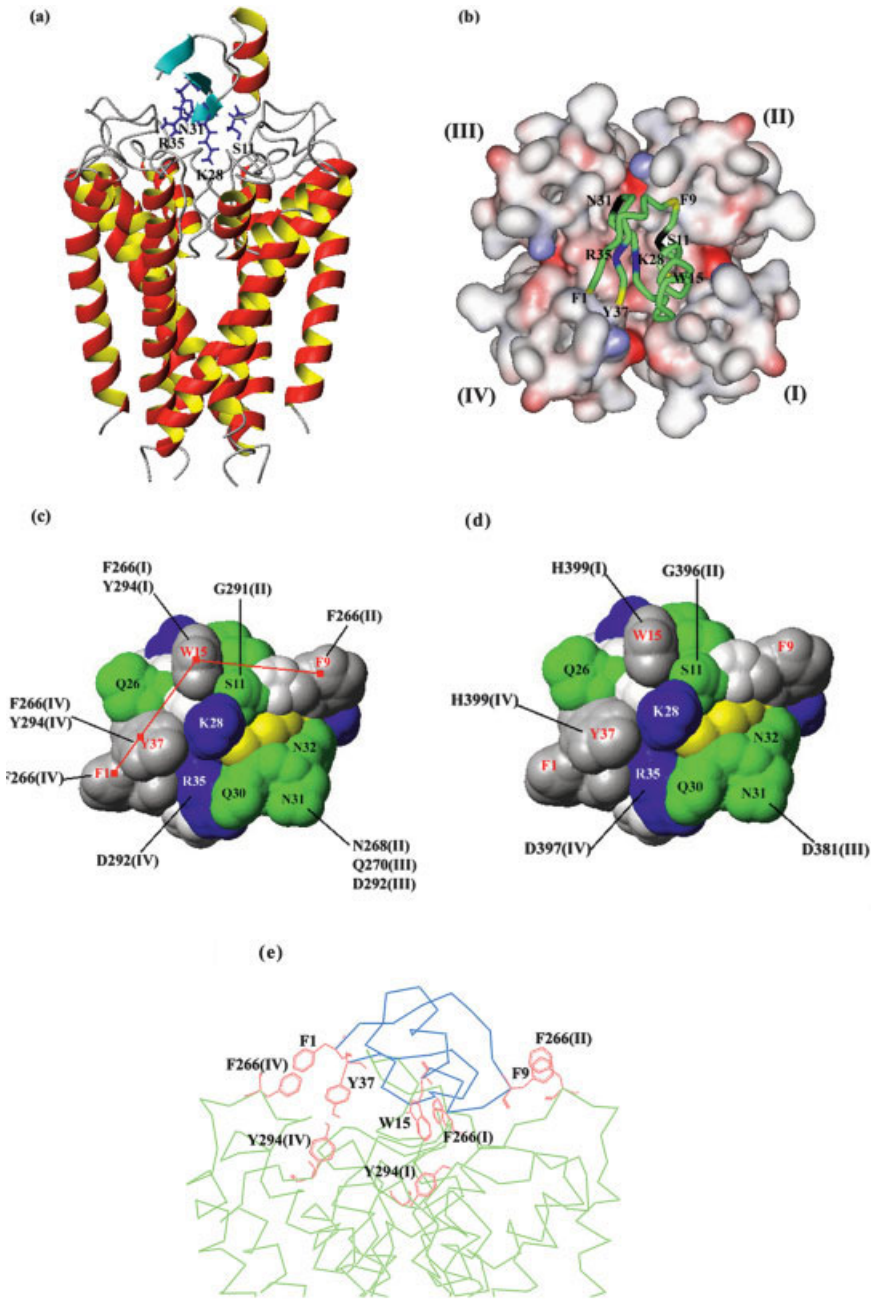

Fig. 5. (**a**) The front view of the BmTx3B–Kca1.1 channel complex generated by MOLMOL. The residues, Lys28 and Arg35, which have formed hydrogen bonds with the residues of the channel, are marked. (**b**) The top view of the BmTx3B–Kca1.1 channel complex generated by the program WebLab ViewerPro 4.0. The Kca1.1 channel is represented as a molecular surface colored by electrostatic potential, and BmTx3B as a green tube structure. (**c** and **d**) Interaction interfaces of BmTx3B with Kca1.1. (right) and Kv1.3 (left). The key interactions pairs are indicated with black lines, while, for clarity, the interactions between Lys28 of BmTx3B and Tyr290 (I–IV) of the Kca1.1 channel and Tyr395 (I–IV) of the Kv1.3 channel are not shown. Blue, yellow, green, white, and gray surfaces represent basic, sulfur-containing, polar, nonpolar, and aromatic residues, respectively. The red quadrate lines highlight the peptide residues involved in π–π or hydrophobic core interactions. (**e**) Aromatic clusters in the complex of BmTx3B (blue) and Kca1.1 channel (green). The residues predicted to form the π–π stacking clusters are shown as red line models.

about 3 orders of magnitude destabilized binding with Kca1.1 channel. Gao and Garcia[29] demonstrated that in the model of ChTx–Kca1.1 complex, the pairs of aromatic residues Trp14–Tyr294 (I) and Tyr36–Phe266 (III) form the π–π stacking, which contribute substantially to the binding of the peptide. A similar situation also occurs in the model the of IbTx–Kca1.1 complex.[29] Therefore, a network of aromatic π–π stackings be-

TABLE II. Observed Interactions Between the BmTX3B Scorpion Toxin and the Kca1.1 Channel in the BmTx3B–Kca1.1 Channel Complex

Observed hydrogen bonds between BmTX3B and Kca1.1 channel

Scorpion toxin BmTX3B		Kca1.1 channel		
Residue	Atom	Residue[a]	Atom	Distance (Å)
Phe9	O	Asn269 (II)	N	2.93
Ser11	OG	Gly291 (II)	O	2.95
Lys28	NZ	Tyr290 (I)	O	2.81
Lys28	NZ	Tyr290 (II)	O	2.85
Lys28	NZ	Tyr290 (III)	O	2.88
Lys28	NZ	Tyr290 (IV)	O	2.86
Gln30	NE2	Gln267 (III)	O	3.24
Asn31	O	Asn268 (II)	ND2	2.90
Asn31	ND2	Gln270 (III)	OE1	3.00
Asn31	N	Asp292 (III)	O	3.20
Arg35	NH2	Asp292 (IV)	OD1	3.01
Tyr37	OH	Asn269 (IV)	N	3.15

Observed hydrophobic contacts between BmTX3B and Kca1.1 channel

Scorpion toxin BmTX3B	Kca1.1 channel
Phe1	Phe266 (IV)
Phe1	Asn269 (IV)
Phe9	Phe266 (II)
Phe9	Asn268 (II)
Trp15	Phe266 (I)
Trp15	Tyr294 (I)
Asn32	Phe266 (II)
Tyr37	Phe266 (IV)
Tyr37	Asn268 (IV)
Tyr37	Tyr294 (IV)

[a]I, II, III, and IV represent the 4 chains of the Kca1.1 channel.

tween BmTx3B and Kca1.1 channel is predicted to contribute substantially to the higher affinity of BmTx3B to Kca1.1 channel, as shown in Figure 5(e).

Rationalization of the Kinetic Behaviors of BmTx3B to Kca1.1 Channel

The kinetic behaviors of BmTx3B blocking Kca1.1 channel were compared with those of ChTx by biosensor binding assay.[24] The results revealed that the association and dissociation rate constants of BmTx3B binding to rat synaptosomes are $1.67 \times 10^4\ M^{-1}\ s^{-1}$ and $5.5 \times 10^{-6}\ s^{-1}$, respectively. They are about 10^4 times lower than those of ChTx ($7.5 \times 10^8\ M^{-1}\ s^{-1}$ and $1.95 \times 10^{-2}\ s^{-1}$, respectively). This kind of kinetic behavior of BmTx3B could be related to the structural features of interface between BmTx3B and Kca1.1 channel.

Recently, Sabatier and coworkers[34] suggested a 2-level toxin-binding pictorial view for the interaction of Pi1 toxin and Kv1.2 channel. According to the proposal, the toxin basic ring first acts (via electrostatic forces) in the recognition, interaction, and correct positioning of toxin on to the channel, and then a tighter interaction takes place through, both hydrophobic forces and hydrogen bonding. In present case, only 2 basic residues, Lys28 and Arg35, take part into the recognition and positioning processes between the toxin and Kca1.1 channel. Thus, the association rate should be much slower than that of ChTx–Kca1.1 channel interaction, where a ring of 5 basic residues may be involved in the recognition and positioning processes. On the other hand, as discussed above, the interface of BmTx3B and Kca1.1 channel contains an extra 2 aromatic π–π stacking interactions, which make tight bonding between the toxin and the channel as compared with ChTx toxin. Hence, the disassociation rate of BmTx3B with Kca1.1 channel must be slower.

The interaction mode derived from the docking experiments could be rationalized as the affinity and the distinctive kinetic behavior of BmTx3B toward Kca1.1 channel, but these theoretical results remain to be further validated experimentally.

Finally, Tytgat and coworkers[36] have reported that 2 separate functional faces might exist on the BmTx3 (αKTx15.2 or BmTx3A) molecule responsible for the 2 different K^+ current-blocking functions. Face A, composed of Arg18 and Lys19 in the α-helix side, might correspond to HERG blocking activity, while Face B, containing a putative functional dyad (Lys27 and Tyr36) in the β-sheet side, might correspond to A type blocking activity. As described previously, BmTx3B toxin also has two faces (Face A, including 2 basic residues, Lys 19 and Lys20, in the α-helix, and Face B, composed of a putative functional dyad, Lys28 and Tyr37, in the β-sheet) that are very similar to those of BmTx3. Therefore, whether BmTx3B is also an α-KTx peptide having HERG blocking activity like that of BmTx3 peptide is a subject for further study. [The atomic coordinates of the 25 energy-minimized conformers used to represent the solution structure of BmTx3B have been deposited in the Brookhaven Data Bank, together with the input of conformational restrains used for the structure calculation under accession No. 1M2S.]

ACKNOWLEDGMENTS

Our thanks to the Institute of Molecular Biology and Biophysics, ETH-Hönggerberg, Zürich, Switzerland, for providing the programs DYANA (version 1.5) and XEASY; to Prof. Bertini of Florence University, Italy, for providing the program CALIBA; and to Prof. James W. Caldwell of the University of California, San Francisco, for providing the program AMBER. We also thank Tripos, Inc., for the Sybyl6.3 software package.

REFERENCES

1. Possani LD, Becerril B, Delepierre M, Tytgat J. Scorpion toxins specific for Na^+-channels. Eur J Biochem 1999;264:287–300.
2. Olamendi-Portugal T, Gomez-Lagunas F, Gurrola GB, Possani LD. A novel structural class of K^+ channel blocking toxin from the scorpion *Pandinus imperator*. Biochem J 1996;315:977–981.
3. Tytgat J, Chandy KG, Garcia ML, Gutman GA, Martin-Eauclaire MF, Van der Walt JJ, Possani LD. A unified nomenclature for short-chain peptides isolated from scorpion venoms: alpha-KTx molecular subfamilies. Trends Pharmacol Sci 1999;20:444–447.
4. Goudet C, Chi C-W, Tytgat J. An overview of toxins and genes from the venom of the Asian scorpion *Buthus martensi* Karsch. Toxicon 2002;40:1239–1258.
5. Batista CVF, Gomez-Lagunas F, Rodriguez de la Vega RC, Hajduc

P, Panyi G, Gaspar R, Possani LD. Two novel toxins from the Amazonian scorpion *Tityus cambridgei* that block Kv1.3 and Shaker B K^+-channels with distinctly different affinities. Biochim Biophys Acta 2002;1601:123–131.
6. Cai Z, Xu CQ, Xu YQ, Lu WY, Chi C-W, Shi YY, Wu JH. Solution structure of BmBKTx1, a new BKca channel blocker from the Chinese scorpion *Buthus martensi* Karsch. Biochemistry 2004;43: 3764–3771.
7. Rodriguez de la Vega RC, Merino E, Becerril B, Possani LD. Novel interactios between K^+ channels and scorpion toxins. Trends Pharmacol Sci 2003;24:222–227.
8. Xu CQ, Zhu SY, Chi CW, Tytgat J. Turret and pore block of K+ channels: what is the difference? Trends Pharmacol Sci 2003;24: 446–448.
9. Jouirou B, Mosbah A, Visan V, Grissmer S, M'Barek S, Fajloun Z, Van Rietschoten J, Devaux C, Rochat H, Lippens G, El Ayeb M, De Waard M, Mabrouk K, Sabatier JM. Cobatoxin 1 from *Centruroides noxius* scorpion venom: chemical synthesis, three-dimensional structure in solution, pharmacology and docking on K+ channels. Biochem J 2004;377:37–49.
10. Rodriguez de la Vega RC, Possani LD. Current views on scorpion toxins specific for K^+-channels. Toxicon 2004;43:865–875.
11. Mouhat S, Jouirou B, Mosbah A, De Waard M, Sabatier JM. Diversity of folds in animal toxins acting on ion channels. Biochem J 2004;378:717–726.
12. Li HM, Wang DC, Zeng ZH, Jin L, Hu RQ. Crystal structure of an acidic neurotoxin from scorpion *Buthus martensii* Karsch at 1.85 Å resolution. J Mol Biol 1996;261:415–431.
13. Wu HM, Wu G, Huang XL, He FH, Jiang SK. Purification, characterization and structural study of the neuro-peptides from scorpion *Buthus martensi* Karsch. Pure Appl Chem 1999;71:1157–1162.
14. Blanc E, Romi-Lebrun R, Bornet O, Nakajima T, Darbon H. Solution structure of two new toxins from the venom of the Chinese scorpion *Buthus martensi* Karsch blockers of potassium channels. Biochemistry 1998;37:12412–12418.
15. Renisio JG, Romi-Lebrun R, Blanc E, Bornet O, Nakajima T, Darbon H. Solution structure of BmKTX, a K^+ blocker toxin from the Chinese scorpion *Buthus martensi*. Proteins 2000;38:70–78.
16. Wu G, Li YM, Wei DS, He FH, Jiang SK, Hu GY, Wu HM. Solution structure of BmP01 from the venom of scorpion *Buthus martensii* Karsch. Biochem Biophys Res Commun 2000;276:1148–1154.
17. Xu YQ, Wu JH, Pei JM, Shi YY, Ji YH, Tong QH. Solution structure of BmP02, a new potassium channel blocker from the venom of the Chinese scorpion *Buthus martensi* Karsch. Biochemistry 2000;39:13669–13675.
18. Zhang NX, Li MH, Chen X, Wang YF, Wu G, Hu GY, Wu HM. Soulution structure of BmKK2, a new potassium channel blocker from the venom of Chinese scorpion *Buthus martensi* Karsch. Proteins 2004;55: 835–845.
19. Escoubas P, Romi-Lehrun R, Lebrun B, Herrmann R, MoskowtL H, Rajendra W, Hammock B, Nakajima T. Tamulotoxin, a novel number of the potassium channel active short toxins from the venom of the Indian red scorpion *Buthus tamulus*. Toxicon 1997;37:806.
20. Marshall DL, Vatanpour H, Harvey AL, Boyot P, Pinkasfeld S, Doljansky Y, Bouet F, Menez A. Neuromuscular effects of some potassium channel blocking toxins from the venom of the scorpion *Leiurus quinquestriatus* hebreus. Toxicon 1994;32:1433–1443.
21. Gimenez-Gallego G, Navia MA, Reuben JP, Katz GM, Kaczorowski GJ, Garcia ML. Purification, sequence, and model structure of charybdotoxin, a potent selective inhibitor of calcium-activated potassium channels. Proc Natl Acad Sci USA 1988;85: 3329–3333.
22. Galvez A, Gimenez-Gallego G, Reuben JP, Roy-Contancin L, Feigenbaum P, Kaczorowski GJ, Garcia ML. Purification and characterization of a unique, potent, peptidyl probe for the high conductance calcium-activated potassium channel from venom of the scorpion *Buthus tamulus*. J Biol Chem 1990;265:11083–11090.
23. Li MH, Wang YF, Chen XQ, Zhang NX, Wu HM, Hu GY. BmTx3B, a novel scorpion toxin from *Buthus martensi* Karsch, inhibits delayed rectifier potassium current in rat hippocampal neurons. Acta Pharmacol Sin 2003;24:1016–1020.
24. Ji YH, Wang WX, Ye JG, He LL, Li YJ, Yan YP, Zhou Z. Martentoxin, a novel K+-channel-blocking peptide: purification, cDNA and genomic cloning, and electrophysiological and pharmacological characterization. J Neurochem 2003;84:325–335.
25. Zhang NX, Wu G, Wang YF, Wang ZH, Feng CL, Wu HM. Purification and primary structure of a toxin-like peptide BmK622 from the venom of Chinese scorpion *Buthus martensii* Karsch. Acta Chim Sin 2003;61:630–634.
26. Wüthrich K. NMR of proteins and nucleic acid. New York: Wiley; 1986. 292 p.
27. Morita T, Hanaoka K, Morales MM, Montrose-Rafizadeh C, Guggino WB. Cloning and characterization of maxi K+ channel alpha-subunit in rabbit kidney. Am J Physiol 1997;273:F615–F624.
28. Doyle DA, Morais Cabral J, Pfuetzner RA, Kuo A, Gulbis JM, Cohen SL, Chait BT, Mackinnon R. The structure of the potassium channel: molecular basis of K^+ conduction and selectivity. Science 1998;280:69–77.
29. Gao YD, Garcia ML. Interaction of agitoxin2, charybdotoxin, and iberiotoxin with potassium channels: selectivity between voltage-gate and maxi-K channels. Proteins 2003;52:146–154.
30. Jones TA, Zhou JY, Cowan, SW, Kjeldgaard M. Improved methods for building protein models in electron density maps and the location of errors in these models. Acta Crystallogr A 1991;47:110–119.
31. Bontems F, Gilquin B, Roumestand C, Menez A, Toma F. Analysis of side-chain organization on a refined model of charybdotoxin: structural and functional implications. Biochemistry 1992;31: 7756–7764.
32. Renisio JG, Lu Z, Blanc E, Jin W, Lewis JH, Bornet O, Darbon H. Solution structure of potassium channel-inhibiting scorpion toxin Lq2. Proteins 1999;34:417–426.
33. Wallace AC, Laskowski RA, Thornton JM. LIGPLOT: a program to generate schematic diagrams of protein–ligand interactions. Protein Eng 1995;8:127–134.
34. Mouhat S, Mosbah A, Visan V, Wulff H, Delepierre M, Darbon H, Grissmer S, De Waard M, Sabatier JM. The "functional" dyad of scorpion toxin Pi1 is not itself a prerequisite for toxin binding to the voltage-gated Kv1.2 potassium channels. Biochem J 2004;377: 25–36.
35. Stampe P, Kolmakova-Partensky L, Miller C. Intimations of K^+ channel structure from a complete functional map of the molecular surface of charybdotoxin. Biochemistry 1994;33:443–450.
36. Huys I, Xu C-Q, Wang C-Z, Vacher H, Martin-Eauclaire M-F, Chi C-W, Tytgat J. BmTx3, a scorpion toxin with two putative functional faces separately active on A-type K^+ and HERG currents. Biochem J 2004;378:745–752.